Structure of AgI-Ag_2O-$2B_2O_3$ glasses: A neutron and x-ray-diffraction investigation

J. Swenson* and L. Börjesson
Department of Applied Physics, Chalmers University of Technology, S-412 96 Göteborg, Sweden

R. L. McGreevy
Studsvik Neutron Research Laboratory, S-611 82 Nyköping, Sweden

W. S. Howells
Rutherford-Appleton Laboratory, Chilton, Didcot, OX11 0QX, United Kingdom

(Received 5 December 1996)

The structures of fast ion conducting glasses in the system $(AgI)_x$-$(Ag_2O\text{-}2B_2O_3)_{1-x}$ have been investigated using x-ray- and neutron-diffraction techniques. The contrasting scattering cross sections of the two techniques for the different atomic species, where the x rays reveal predominantly the Ag and I structural correlations, whereas mainly the boron-oxygen structure is observed with the neutrons, allow for a relatively detailed structural determination of these complex materials. The neutron data show that the short-range order of the boron-oxygen network, which determines the network connectivity, is unaffected by the AgI doping. The silver and iodine ions enter voids in the boron-oxygen network structure. The experimental data also show the existence of considerable intermediate-range ordering which increases with increasing AgI doping. This is manifested in a diffraction peak at low Q (around 0.8 $Å^{-1}$), which grows with increasing AgI content and which is particularly strong in the neutron data. The contrasting results of the x-ray- and neutron-diffraction experiments show unambiguously that this ordering is mainly due to correlations within the boron-oxygen network. The experimental data have been used for structural modeling using the reverse Monte Carlo method. Structural models have been produced which are simultaneously in accordance with both the x-ray and the neutron data, as well as with the experimental density. The simulations show that the intermediate-range ordering is due to interchain ordering between neighboring chain segments. Analysis of the models shows that most silver ions are coordinated to both iodine and oxygen ions of negatively charged BO_4 units in the network. This observation, as well as the evidence that the intermediate-range ordering observed is due to the boron-oxygen network, excludes the presence of any significant amount of AgI clusters, which have been suggested in the literature to be responsible for the high ionic conductivity of AgI-doped oxyglasses. Instead the results support the idea that the silver and iodine ions expand the network which open doorways and creates new pathways in the structure suitable for ion conduction. [S0163-1829(97)04817-0]

I. INTRODUCTION

Glasses with high ionic conductivity presently attract considerable scientific interest because of their potential applications as solid electrolytes in electrochemical devices such as solid-state batteries, fuel cells, chemical sensors, and ''smart windows.'' Typical fast ion conductors are metal-oxide modified borate and phosphate glasses doped with metal halide salts. They have become model materials for investigation of the conduction mechanism in amorphous ionic conductors because of their high ionic conductivity, wide glass range, ease of glass formation, and chemical stability.

In the case of borate glasses the addition of metal oxide considerably modifies B_2O_3, which is a strong glass former in Angell's classification,[1–3] and gives a partially ionic character by accommodation of the oxygen atoms into the glassy network structure. In this way the number of three-coordinated boron atoms, typical of pure B_2O_3, decreases while tetrahedral BO_4 units are formed.[4,5] The ionic conductivity, associated with the mobility of the M^+ ions, increases drastically with increasing concentration of the metal-oxide and room-temperature conductivities of 10^{-7} S/cm can be obtained.[6] Even higher conductivities can be achieved by dissolving a metal halide salt (e.g., LiI, LiCl, AgI, AgBr, etc.) into the metal-oxide modified glass, which can raise the conductivity up to 10^{-2} S/cm at room temperature.[6] The introduction of the dopant salt does not seem to affect the local structure of the B-O network as indicated by Raman and NMR results,[4–7] and it has been proposed that the ions of the dopant salt occupy interstices in the glassy structure and that they are only weakly connected to the glass network.[4,7–9] However, the host glass network expands considerably to accumulate the dopant ions and large changes of the intermediate structure are indicated by neutron-diffraction experiments.[8,9] This may be of importance for the high conductivities of the metal halide doped glasses.

Despite considerable experimental and theoretical efforts the conductivity mechanism is not yet fully understood.[10] This is partly due to an incomplete knowledge of the microscopic structure from the available experimental results, in particular, on the important intermediate length scale, i.e., 4-50 Å, where correlations between various structural subunits may be significant. Models based on various hypothetical microscopic structures have been proposed to explain the high conductivities of metal halide doped glasses. In one

kind, the cluster model,[11–17] it is proposed that the metal halide salt is introduced into the amorphous network in clusters or microdomains of size >10 Å. Within the microdomains, which are assumed to have an internal structure similar to that of the dopant salt, the barriers for conduction are low whereas there may be relatively large barriers between clusters. This model has been used particularly to explain the high ionic conductivity in AgI-doped glasses. AgI is, in its crystalline α phase above 147 °C, one of the best ionic conductors known. In another kind of model the ionic conductivity takes place within connected conduction pathways of relatively low activation barriers.[7,18,19] This idea was first proposed to explain the conductivity of metal-oxide modified oxide glasses and has later been extended in various forms to the salt-doped glasses. The pathways are then assumed to be formed by the anions of the dopant salt and/or the negatively charged centers of the network, e.g., the BO_4^- groups. There are also various models which rest on the assumption that the ions of the dopant salt are homogeneously distributed in the glass. Two of these are the ''random site model'' (Ref. 20) and the weak electrolyte model.[21] Although they make the same structural assumption these models are distinctly different. For example, in the random site model the role of the dopant salt is, apart from providing the charge carriers, to lower the potential barriers within the glass. All cations are assumed to contribute to the conductivity. Thus, it is mainly the mobility of the cations which increases with increasing dopant salt concentration. In the weak electrolyte model,[21] the mobility is independent of the glass composition and the change in conductivity with glass composition is completely due to a change in the number of charge carriers. It is proposed that only a fraction of the cations contribute to the conduction, all the remainder are fixed and associated with the glass network. In yet another model Tuller and Button[22] have suggested that the increase in conductivity with increasing cation concentration is simply due to the dopant salt expanding the glass network, resulting in a more open structure suitable for ion conduction.

The diversity of specific assumptions in the various models of the microscopic structural properties of the glasses emphasizes the need for a better understanding of the microscopic structure. In this paper, we have used x-ray- and neutron-diffraction (including isotope substitution of Ag) techniques in combination with the reverse Monte Carlo (RMC) modeling[23,24] to investigate the structure of a model system for fast ion conducting glass systems, namely $(AgI)_x(Ag_2O\text{-}2B_2O_3)_{1-x}$ ($x=0-0.6$). In view of the assumptions of the structural and conductivity models discussed above, it is of particular interest to investigate the environment around the Ag^+ ions and the structural origin of a strong diffraction peak previously observed by neutron diffraction at an anomalously low-Q value of about 0.8 $Å^{-1}$,[8,9] which indicates intermediate-range ordering on a length scale of about 8 Å. A similar peak has also been observed in other AgI-doped glasses.[25,26] The nature of the associated intermediate-range ordering has been a matter of controversy (see, for example, Refs. 17 and 27). In this paper we show that the origin of the prepeak in AgI-doped borate glasses is predominantly due to local-density fluctuations of the B-O network structure.

II. DIFFRACTION NOTATION

A. Neutron diffraction

We will use the following notation for the scattered neutron intensity from glasses and for the corresponding real-space functions. The differential scattering cross section $I(Q)$ $(=d\sigma/d\Omega)$ can be expressed as a sum of two terms:[28]

$$I(Q)=I_s+I_D=\sum_i c_i\langle b_i^2\rangle[1+P_i(Q,\theta)] + \frac{1}{Q}\int_0^\infty D(r)\sin(Qr)dr, \quad (1)$$

where the first term is known as the self-scattering and the second term is known as the distinct scattering. It is the latter which carries information on the interatomic correlations. The summation is taken over the different elements in the sample, c_i is the fraction of i atoms in the sample, and $\langle b_i^2\rangle$ is the mean-squared scattering length for element i. $D(r)$ is the neutron-weighted reduced pair distribution function and $P_i(Q,\theta)$ represents inelastic-scattering events and is known as the Placzek correction term.[28] The static structure factor, $S(Q)$, is obtained from the distinct scattering as follows:

$$S(Q)=\frac{I_D(Q)}{\Sigma_i c_i\langle b_i\rangle^2}+1. \quad (2)$$

$D(r)$ is obtained by Fourier transformation of the distinct scattering:

$$D(r)=\frac{2}{\pi}\int_0^\infty QI_D(Q)\sin(rQ)dQ. \quad (3)$$

$D(r)$ can also be written as the neutron-weighted (i.e., dependent upon the scattering lengths of the constituent atoms) sum of the reduced partial pair distribution functions $d_{ij}(r)$:

$$D(r)=\sum_{i,j} c_ic_jb_ib_jd_{ij}(r). \quad (4)$$

Let us here also define the atomic pair correlation function, $G(r)$, which is obtained from $D(r)$ through

$$G(r)=D(r)\Big/4\pi\rho r\left(\sum_i c_ib_i\right)^2+1, \quad (5)$$

where ρ is the atomic number density.

B. X-ray diffraction

A general theory for x-ray scattering can be found in Ref. 29. Here we will use a notation for x-ray diffraction which is similar to that for neutron diffraction, with the exception of the scattering length (denoted b for neutrons), which here is Q dependent and given by the atomic form factor, $f_i(Q)$, for element i. It is also important to note that the Q dependences of the partial atomic form factors are different. Hence, a formally correct correspondence to Eq. (1) can for x rays only be made for a one-component system, where the scattered intensity is given by

$$I(Q)=I_s+I_D=f^2(Q)+\frac{1}{Q}\int_0^\infty D(r)\sin(Qr)dr. \quad (6)$$

The normalized structure factor, $F(Q)$, is obtained from $I(Q)$ through

$$F(Q)=I(Q)/I_s. \quad (7)$$

For an n-component system the total structure factor $F(Q)$ can be expressed as a sum of the Faber-Ziman partial structure factors $S_{ij}(Q)$:[30]

$$F(Q)=\frac{\Sigma_{i,j=1}^{n} c_i c_j f_i(Q) f_j(Q)[S_{ij}(Q)-1]}{\Sigma_{i=1}^{n} c_i f_i(Q)^2}+1. \quad (8)$$

Thus, it is not possible to obtain a correct total $G(r)$ by a direct Fourier transformation of $F(Q)$ for a multicomponent system, since the form factors of different chemical components do not have the same Q dependence.

III. EXPERIMENT

A. Neutron diffraction

Ion conducting glasses with compositions $(AgI)_x$-$(Ag_2O\text{-}2B_2O_3)_{1-x}$($x=0$–0.6) were prepared using a conventional melt-quenching method according to procedures described previously.[31,32] In all samples boron was isotopically enriched in ^{11}B (99%) in order to minimize the influence of the high neutron absorption of ^{10}B present in natural boron. For the AgI-Ag_2O-$2B_2O_3$ composition an additional sample with ^{107}Ag (instead of natural silver) was prepared. The samples, which were in shapes of cylindrical rods with a diameter of 9 mm and a length of 50 mm, were mounted in thin-walled vanadium containers. The neutron-diffraction experiments were performed on the time-of-flight liquid and amorphous materials diffractometer (LAD) at the pulsed neutron source ISIS, Rutherford Appleton Laboratory. The diffractometer has been described in detail elsewhere.[33] Time-of-flight spectra were recorded separately for each group of detectors at the angles 150°, 90°, 58°, 35°, 20°, 10°, and 5° and also for monitors in the incident and transmitted beam, respectively. The data of each detector group were corrected separately for background and container scattering, absorption, multiple-scattering, and inelasticity effects, and normalized against the scattering of a vanadium rod following the procedure in Refs. 34 and 35. The corrected individual data sets obtained at each angle were then combined in order to obtain a large-Q range and to improve the statistics. For each data set only the Q range that agreed with other data sets in the overlapping Q region was used. Preliminary results for the Ag_2O-$2B_2O_3$ and $(AgI)_{0.6}(Ag_2O\text{-}2B_2O_3)_{0.4}$ samples have been presented in earlier reports;[8,9] however a less accurate data correction procedure was used in those reports.

B. X-ray diffraction

X-ray-diffraction experiments on $(AgI)_x(Ag_2O\text{-}2B_2O_3)_{1-x}$ ($x=0$, 0.6) were performed at Station 9.1,[36] a high-precision powder diffractomer situated at the SERC's Synchrotron Radiation Source (SRS), Daresbury Laboratory, UK. The glass samples were powdered and stuck on tapes.

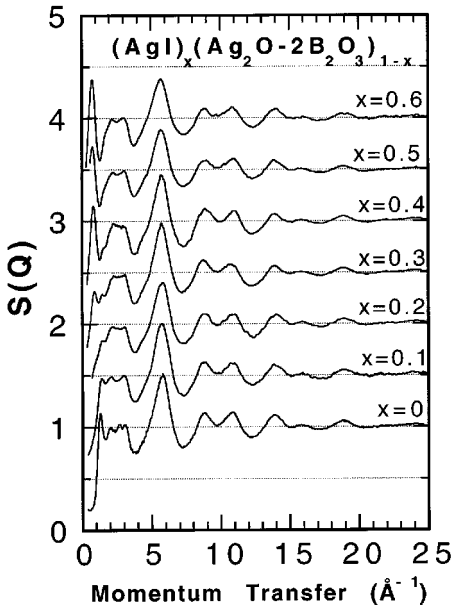

FIG. 1. Experimental neutron structure factors, $S(Q)$, for the glasses $(AgI)_x(Ag_2O\text{-}2B_2O_3)_{1-x}$ ($x=0$–0.6). The upper curves have been shifted in subsequent steps of 0.5.

Measurements were made in transmission geometry for $2°<2\theta<22°$ and reflection geometry for $10°<2\theta<120°$. The x-ray wavelength was 0.689 Å. After separate corrections the two spectra were scaled to overlap in the region $10°<2\theta<20°$ and combined. The inelastic Compton scattering[37] was subtracted experimentally using the Warren-Mavel method[38] (Zr K edge), as developed for use on Station 9.1.[39] The data were also corrected for scattering from the tape, absorption, and polarization, divided by the total atomic form factor and normalized to unity at large scattering angles. Multiple scattering was assumed to be negligible.

IV. RESULTS OF THE EXPERIMENTS

A. Neutron diffraction

The neutron structure factors, $S(Q)$, of $(AgI)_x(Ag_2O\text{-}2B_2O_3)_{1-x}$ ($x=0$–0.6) are shown in Fig. 1. It should be noted that the total number density is dominated by boron and oxygen for all the investigated glasses (see Table I) and that the scattering lengths of the atomic species are of the

TABLE I. Number densities for $(AgI)_x$-$(Ag_2O\text{-}2B_2O_3)_{1-x}$ ($x=0$–0.6) glasses are shown. Both the total number densities and the separate number densities for boron + oxygen and silver + iodine are given.

Glass composition	Number densities (atoms/Å^3)		
	Total	B+O	Ag+I
$x=0$	0.0846	0.0716	0.0130
$x=0.1$	0.0852	0.0709	0.0143
$x=0.2$	0.0824	0.0671	0.0153
$x=0.3$	0.0790	0.0627	0.0163
$x=0.4$	0.0759	0.0582	0.0177
$x=0.5$	0.0705	0.0517	0.0188
$x=0.6$	0.0642	0.0441	0.0201

TABLE II. Weighting factors for the different atomic pair correlations in neutron- and x-ray-diffraction experiments of Ag_2O-$2B_2O_3$. The ratios between the neutron and x-ray weighting factors are also given.

	Weighting factors Ag_2O-$2B_2O_3$		
Atom pair	Neutron	X ray	Ratio Neutron/x ray
B-B	0.1117	0.0138	0.124
B-O	0.3439	0.0776	0.226
B-Ag	0.1012	0.1301	1.286
O-O	0.2650	0.1086	0.401
O-Ag	0.1554	0.3643	2.344
Ag-Ag	0.0228	0.3056	13.40

same order. This implies that the total scattering is dominated by boron-oxygen correlations (see Tables II and III). From the figure it is evident that all the glasses show almost identical results for the high-Q range, indicating very similar short-range B-O structures. The insensitivity of the high-Q range to metal halide doping then support previous Raman, NMR, and neutron-diffraction results[4,7–9] indicating that the ions of the dopant salt do not participate in the network formation, rather they enter into interstices and voids of the host B-O network structure. However, in the low-Q region below 3 $Å^{-1}$ there are clear differences between the investigated glasses. The first (sharp) diffraction peak (FSDP), at 1.3 $Å^{-1}$ for the undoped glass decreases in intensity with increasing AgI concentration and, instead, a new prepeak at about 0.8 $Å^{-1}$ successively grows in intensity. The prepeak, which appears as a shoulder for the composition $x=0.2$, is first seen as a resolved peak for $x=0.3$ and for the highest AgI concentration the peak has grown considerably and the amplitude is as high as that of the main peak of $S(Q)$ at about 6 $Å^{-1}$. The position of this low-Q peak, Q_1, corresponds to a real-space characteristic length of about $2\pi/Q_1 \approx 8$ Å. Thus, the introduction of AgI induces longer length-scale density fluctuations than those of the undoped glass.

TABLE III. Weighting factors for the different atomic pair correlations in neutron- and x-ray-diffraction experiments of the $(AgI)_{0.6}(Ag_2O$-$2B_2O_3)_{0.4}$ glass and for the difference between the two neutron samples of AgI-Ag_2O-$2B_2O_3$ (^{107}Ag-^{n}Ag). The ratios between the neutron and x-ray weighting factors of the $(AgI)_{0.6}(Ag_2O$-$2B_2O_3)_{0.4}$ glass are also given.

	Weighting factors $(AgI)_x(Ag_2O$-$2B_2O_3)_{1-x}$			
	Neutron			Ratio
Atom pair	$x=0.6$	$x=0.5$ ^{107}Ag-^{n}Ag	X ray $x=0.6$	X ray/neutron $x=0.6$
B-B	0.0746	0	0.0039	0.0523
B-O	0.2325	0	0.0219	0.0942
B-Ag	0.1195	0.282	0.0642	0.537
B-I	0.0451	0	0.0311	0.690
O-O	0.1809	0	0.0306	0.169
O-Ag	0.1859	0.439	0.1799	0.968
O-I	0.0704	0	0.0870	1.24
Ag-Ag	0.0479	0.221	0.2643	5.52
Ag-I	0.0362	0.058	0.2554	7.06
I-I	0.0070	0	0.0617	8.81

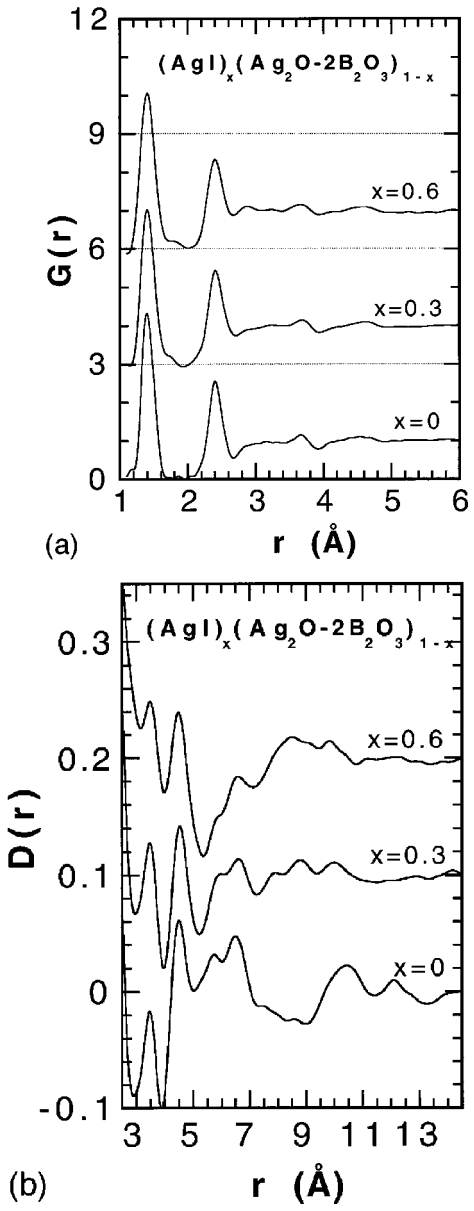

FIG. 2. Neutron weighted atomic pair correlation functions, $G(r)$, (a) and reduced pair distribution functions, $D(r)$, (b) for the glasses $(AgI)_x(Ag_2O$-$2B_2O_3)_{1-x}$ ($x=0$, 0.3, and 0.6). The upper curves have been shifted to higher values for clarity.

We also observe features in the real-space correlations, corresponding to those seen in the structure factors. In Fig. 2(a), which shows the atomic pair correlation functions, $G(r)$, for the compositions $x=0$, 0.3, 0.6, it is evident that the short-range order of the BO network is unaffected by the introduced metal halide salt, since neither the first peak at 1.4 Å (the nearest B-O distance) nor the second peak at 2.4 Å (the nearest B-B and O-O distances) show any significant changes with increasing dopant salt concentration. The only apparent effect of the AgI doping on the short-range corre-

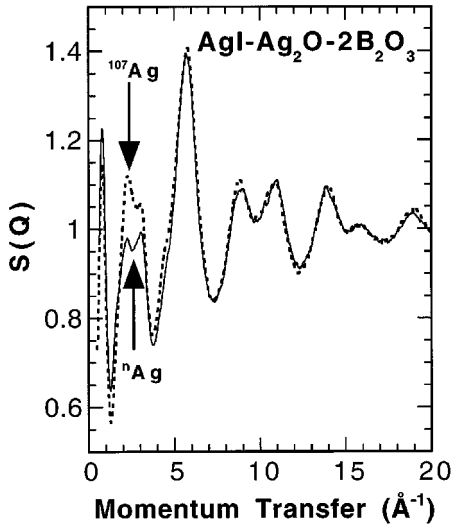

FIG. 3. Experimental neutron structure factors, $S(Q)$, of the two neutron samples (natural Ag and ^{107}Ag) of AgI-Ag_2O-$2B_2O_3$. The dashed line represents the ^{107}Ag sample and the solid line is for the sample with natural Ag.

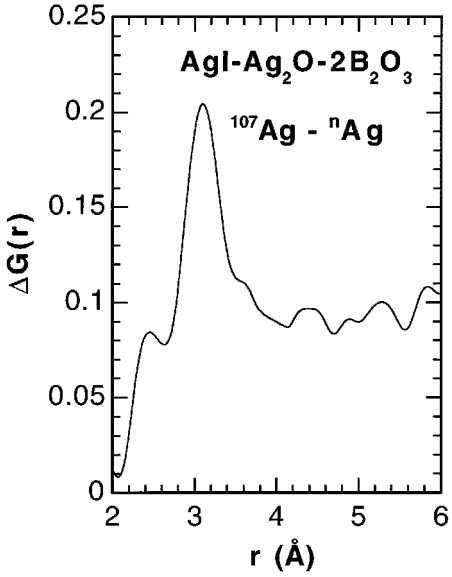

FIG. 4. Shows the difference in $G(r)$ between the two neutron samples of AgI-Ag_2O-$2B_2O_3$ (^{107}Ag-^{n}Ag).

lations is the appearance of a small peak at 2.85 Å. This peak is probably due to the nearest Ag-I distance since it nearly coincides with the Ag-I distance (2.8 Å) in crystalline α-AgI.[40]

The correspondences in real space to the observed differences in the low-Q range of the structure factors are better emphasized in Fig. 2(b), where the reduced pair distribution function $D(r)$ is plotted in the range $2.5<r<14.5$ Å for the compositions $x=0,0.3,0.6$. The figure shows two interesting points. First, all the curves exhibit relatively sharp peaks out to about 10 Å and all these peaks are situated at about the same position in all glasses. These peaks are real and are not spurious features introduced by the Fourier transformation procedure. This was tested by truncating $S(Q)$ at various different $Q_{\max}$ prior to Fourier transformation. The small but relatively well-defined peaks out to about 10 Å indicate considerable internal ordering within the boron-oxygen network, which is similar for all the glasses investigated. They may then be interpreted as characteristic distances within B-O chains or segments. Second, the origin of the FSDP may be seen also in real space. The undoped and highest doped glasses show broad peaks at around 5 and 8.5 Å ($\approx 2\pi/Q_1$), respectively, while the glass with the intermediate AgI concentration ($x=0.3$) exhibits no clearly observable characteristic distance in analogy with the weak FSDP observed in $S(Q)$. The characteristic distances of 5 and 8.5 Å in the undoped and highest doped glasses, respectively, are ''quasiperiodic'' and extend at least to the second-order correlations at about $2r$, which in the figure is seen as a broad weak peak at about 10–11 Å for the undoped glass. Thus, there are real-space features in $D(r)$ out to about 20 Å, corresponding to the observations made for the low-Q range in $S(Q)$, which can be interpreted in terms of intermediate-range ordering phenomena.

The experimental neutron structure factors, $S(Q)$, of the two samples with different silver isotopes (natural Ag and ^{107}Ag) of AgI-Ag_2O-$2B_2O_3$ are shown in Fig. 3. Very similar results are observed over the whole Q range, except for the interval 2–4 Å^{-1}, where the intensity for the sample with ^{107}Ag is much higher. Thus the correlations involving silver contribute mainly in this Q region. It is also interesting to note that the intensity of the prepeak is slightly lower for the sample with ^{107}Ag, showing that silver ions are not directly involved in the correlations giving rise to the FSDP. Rather, the decreasing intensity of the FSDP for increasing Ag scattering length indicates that the Ag contribution to the FSDP is less than the average contribution of the other three (i.e., B, O, and I^-) components.

Figure 4 shows the difference in $G(r)$ between the two silver samples of AgI-Ag_2O-$2B_2O_3$. The relative scattering of the two samples has been weighted so as to cancel all correlations except those involving Ag (see Table III). The small peak at about 2.5 Å in Fig. 4 is attributed to the nearest Ag-O distance as in glassy Ag_2O-$2B_2O_3$ (Ref. 35) and crystalline Ag_2O-$4B_2O_3$.[41] The main peak at 3.1 Å must be due to the nearest Ag-Ag and Ag-B correlations, provided that there is no pronounced Ag-O correlation in the actual r region. Also, contributions from Ag-I correlations are expected in this r range. However, the weighting factor for Ag-I is relatively low (see Table III). It should also be noted that there are no distinct Ag correlations involved beyond 4 Å within the experimental accuracy.

B. Structure factors from x-ray diffraction

The experimental x-ray structure factors of Ag_2O-$2B_2O_3$ and $(AgI)_{0.6}$ $(Ag_2O\text{-}2B_2O_3)_{0.4}$ are shown in Fig. 5(a). The x-ray structure factor of the undoped glass ($x=0$) shows a first diffraction peak at 1.25 Å^{-1}, i.e., at a slightly lower value than in the neutron structure factor, and a strong main peak at 2.25 Å^{-1}, probably related to nearest Ag-Ag correlations considering its strength and the relative scattering contributions of the different atoms (see Table II). Relatively sharp peaks are also observed at about 3.2 and 4.3 Å^{-1}. At higher Q the structure factor shows only a weak oscillation with a period of about 2.5 Å^{-1}. For the AgI-

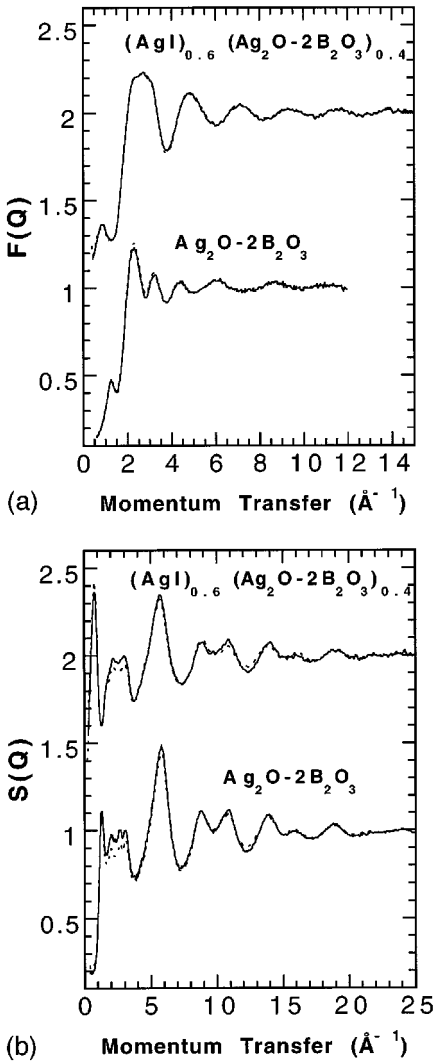

FIG. 5. Experimental x-ray (a) and neutron (b) structure factors (solid lines) and computed x-ray weighted (a) and neutron weighted (b) total structure factors (dashed lines) for the RMC configurations of Ag_2O-$2B_2O_3$ and $(AgI)_{0.6}(Ag_2O$-$2B_2O_3)_{0.4}$. The structure factors of the doped glass have been shifted vertically by one unit.

doped glass ($x=0.6$) a first diffraction peak occurs at 0.85 $Å^{-1}$, i.e., at a slightly higher value than in the neutron structure factor, and the main peak is situated at about 2.7 $Å^{-1}$. Above the main peak only periodic oscillations at multiples of this Q are observed. The structure factor for the $x=0.6$ sample is in good agreement with previously reported x-ray results obtained by Licheri *et al.*[42]

C. Origin of the first sharp diffraction peak

Let us now compare the x-ray-weighted structure factors [see Fig. 5(a)] with the corresponding neutron-weighted structure factors shown in Fig. 5(b). This is interesting, since the atomic scattering coefficients are very different for the present glasses (see Tables II and III). For the undoped glass (see Table II) the total neutron scattering is dominated by correlations within the boron-oxygen network (72%), whereas the x-ray-weighted scattering is dominated by silver correlations (80%). For the AgI-doped glass the difference between the neutron and x-ray structure factors is even greater (see Table III); in the neutron-diffraction experiment the internal boron-oxygen network correlations dominate by a factor of 5 compared to the silver and iodine correlations, whereas in the x-ray-diffraction experiment the total scattering from silver and iodine is more than 10 times larger than from the boron-oxygen network.

Let us focus here on the intermediate-range correlations which mainly contribute to the low-Q range of the respective structure factor. For both the undoped and doped glasses the positions of the respective first diffraction peak are similar in the x-ray and neutron structure factors [see Figs. 5(a) and 5(b)]. The intensities are, however, much lower in the two x-ray structure factors. This difference is then due to the different weighting factors in neutron and x-ray diffraction experiments. The origin of the FSDP is obviously due to density fluctuations in the B-O network, since the x-ray data see predominantly Ag and I correlations, whereas the neutron data are mostly sensitive to O and B correlations.

V. REVERSE MONTE CARLO SIMULATIONS

From the combination of neutron- and x-ray-diffraction experiments we established in the previous section a few of the short-range bond distances and that it is predominantly the B-O network that gives rise to the anomalous FSDP in the AgI-doped glass. However, to obtain a more detailed ''picture'' of the structure it is desirable to perform some kind of modeling of the glass structure. This can be done by using common computer-simulation techniques like molecular dynamics (MD) and Monte Carlo (MC) simulations, but it is a complex task because of the difficulty to obtain sufficiently good interatomic pair potentials for the present complicated glasses. Despite these difficulties MD simulations have been reported recently on glasses with the same composition as in the present study.[43] While the MD study reproduced relatively well the high-Q part of $S(Q)$, there were large discrepancies in the low-Q range of $S(Q)$. We have taken a different approach; we have applied the reverse Monte Carlo (RMC) modeling technique[23,24] in order to make direct use of the available experimental data. The technique, which has recently been successfully applied to other network and fast ion conducting glasses,[24,27] will be applied here to create structural models using the present neutron- and x-ray-diffraction data of the silver borate glasses.

A. The method

RMC uses a standard metropolis Monte Carlo (MMC) algorithm[44] to move particles within the simulation box (Markov chain, periodic boundary conditions, etc.), but instead of minimizing the energy, the squared difference between the experimental structure factor and the structure factor calculated from the computer configuration was minimized. Thus, no interatomic potentials are needed in the RMC method, but instead it requires accurate structural data as input. Data from different sources [neutron, x-ray, extended x-ray-absorption fine structure (EXAFS)] may be simultaneously fitted. Using RMC it is possible to obtain three-dimensional structural models of disordered materials that agree quantitatively with the available diffraction data (provided that the data do not contain significant systematic errors).

B. Simulation procedure

To be able to simulate the intermediate-range structural order the configuration has to be large enough so that the corresponding box size does not influence the ordering in question, i.e., a large number of atoms must be used. The computer configurations of the present undoped ($x=0$) and doped ($x=0.6$) glasses contained 3900 and 3840 atoms, respectively. The box lengths of the undoped and doped glasses were given the values 35.86 and 39.11 Å, respectively, which correspond to the experimentally measured densities. Periodic boundary conditions were used in cubic boxes.

In order to ensure physically realistic configurations, in the sense that there is no overlap of atoms and that the B and O atoms form a proper network, we ran hard-sphere Monte Carlo (HSMC) simulations with certain constraints applied. The constraints were of two kinds; closest atom-atom approach and connectivity. The closest distances that two atoms were allowed to approach were determined from the experimental results, e.g., the radial distribution functions. The following closest atom-atom distances were used in the simulations: 1.25 Å for B-O, 2.1 Å for B-B, O-O and Ag-O, 2.4 Å for Ag-I, 2.5 Å for Ag-Ag, 2.6 Å for Ag-B, 2.8 Å for O-I, 3.2 Å for B-I, and 3.6 Å for I-I. The constraints on the B-O network connectivity were applied on the basis of results obtained by NMR,[4,5] Raman,[45,46] and infrared experiments.[47] These experiments have shown that the addition of M_2O to B_2O_3 causes a progressive increase in the number of four-coordinated borons at the expense of three-coordinated ones. At the composition M_2O-$2B_2O_3$ the fraction of four-coordinated borons is close to 45%. Therefore, we have applied the constraints that all the oxygens are coordinated to two borons and that 45% of the borons are coordinated to four oxygens. The remaining borons are coordinated to three oxygens. The B-O distance was allowed to vary from 1.25 to 1.65 Å. In this way we have ensured that BO_3 and BO_4 units are formed and that they are linked together in a network. After the BO network was produced by the HSMC simulation, all the Ag^+ and I^- ions were randomly added into the computer box. These were then moved apart from each other and from the B and O atoms in order to fulfill the closest atom-atom constraints.

C. Results

The structure factors of $(AgI)_x(Ag_2O\text{-}2B_2O_3)_{1-x}$ ($x=0,0.6$) glasses obtained by RMC modeling are compared with those obtained experimentally in Figs. 5(a) and 5(b). The overall structure factors are well reproduced and, in particular, the first sharp diffraction peak (FSDP) is well fitted in both cases. The configurations should therefore contain information related both to the short-range order and to the origin of the FSDP and the type of intermediate-range order producing it. Some deviations from the experimental neutron structure factors are observed in the Q region around 2–4 $Å^{-1}$. [Smaller deviations are also observed in the high-Q range above 10 $Å^{-1}$ for $(AgI)_{0.6}(Ag_2O\text{-}2B_2O_3)_{0.4}$.] Previous RMC modeling on other materials using data taken on LAD indicate that the range 2–4 $Å^{-1}$ may contain systematic experimental or correction errors. This is probably the main reason for the deviations in this range. However, note that the low-Q part (1.30–3 $Å^{-1}$) of the structure factor of the Ag_2O-$2B_2O_3$ glass contains four FSDP's and that RMC has managed to reproduce all these, although it has been thought that the peaks are due to complex structural units and that the RMC method should not be able to create these units during the fitting procedure. Thus, in contrast to what has been thought, it has been possible to reproduce the complex low-Q range on the basis of a structure whose topology is predefined by the coordination constraints, i.e., without specifically having to build complex units into the structure.

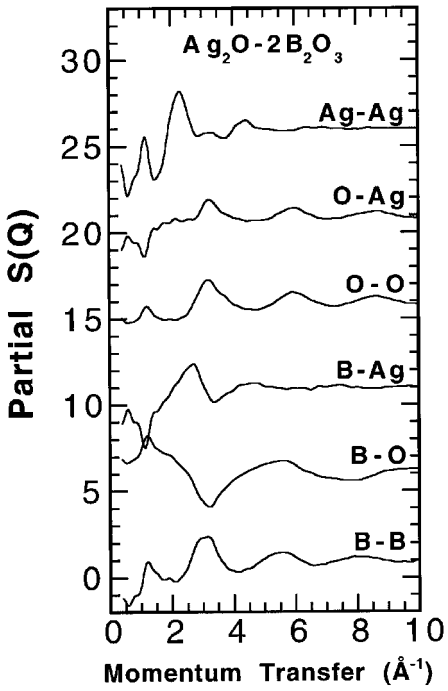

FIG. 6. Partial structure factors, $S_{ij}(Q)$, calculated from the RMC configuration of Ag_2O-$2B_2O_3$. The upper curves have been shifted to higher values for clarity.

The experimental x-ray structure factors are almost exactly reproduced by the RMC configurations. Considering the different weights of the scattering in the x-ray and neutron structure factors and also the excellent agreement of the RMC models with the experimental data, the RMC configurations should contain the essential structural features of the investigated glasses.

1. Intermediate-range order

In Fig. 6 we plot the partial structure factors $S_{ij}(Q)$ of the RMC-produced configuration of Ag_2O-$2B_2O_3$. This confirms the experimental result that the FSDP at 1.3 $Å^{-1}$ is mainly due to correlations within the B-O network. The three partial structure factors $S_{BB}(Q)$,$S_{BO}(Q)$, and $S_{OO}(Q)$ have peaks at about the same Q value (1.2 $Å^{-1}$) as the experimentally observed FSDP. However, it is interesting to note that the other three partial structure factors $S_{Ag\text{-}Ag}(Q)$, $S_{BAg}(Q)$, and $S_{OAg}(Q)$ also show rather well-defined features (dips or peaks) at 1.2 $Å^{-1}$; $S_{Ag\text{-}Ag}(Q)$ has a peak and $S_{BAg}(Q)$ and $S_{OAg}(Q)$ show dips (''negative peaks''), i.e., the correlations are in antiphase to the other four pair corre-

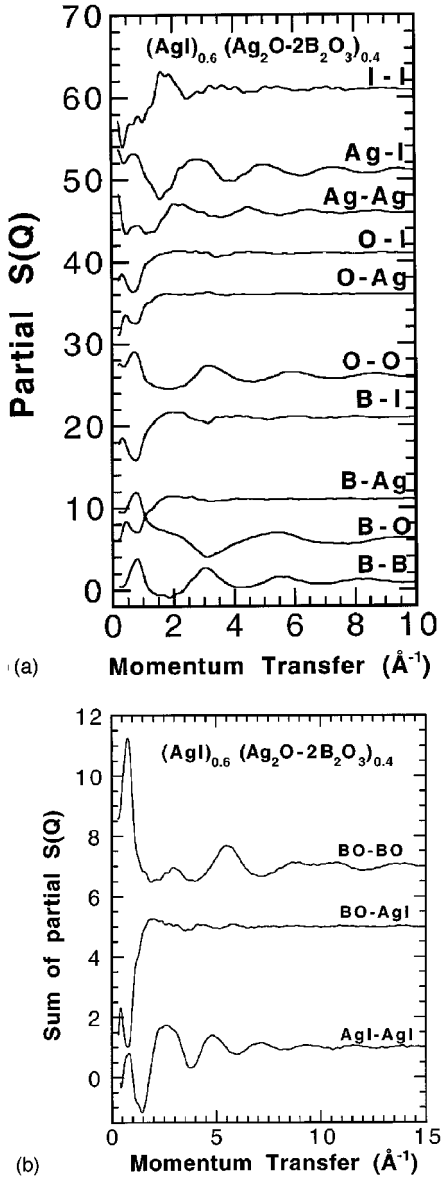

FIG. 7. (a) Partial structure factors, $S_{ij}(Q)$, calculated from the RMC configuration of $(AgI)_{0.6}(Ag_2O\text{-}2B_2O_3)_{0.4}$. (b) The correlations within the BO network (i.e., the B-B, B-O, and O-O), within the AgI salt, and between the network and the salt have been added together to produce the three concentration weighted partial structure factors; BO-BO, AgI-AgI, and BO-AgI, respectively. The upper curves have been shifted to higher values for clarity.

lations, which strongly indicates that the Ag^+ ions crosslink between neighboring BO segments and occupy relatively well-defined positions.

Figure 7(a) shows the partial structure factors of the RMC configuration of $(AgI)_{0.6}(Ag_2O\text{-}2B_2O_3)_{0.4}$. It can be seen that the origin of the FSDP in the total $S(Q)$ is predominantly due to a prepeak at about 0.75 $Å^{-1}$ in the three partial structure factors $S_{BB}(Q)$, $S_{BO}(Q)$, and $S_{OO}(Q)$. We note that the partial $S_{AgI}(Q)$ also shows a broad peak at a similar Q value, however, of relatively low intensity. The partial structure factors which involve correlations between the network atoms and the salt ions [i.e., $S_{AgB}(Q)$, $S_{AgO}(Q)$, $S_{IB}(Q)$, and $S_{IO}(Q)$] have dips at the Q value of the FSDP. This is even more evident in Fig. 7(b), where the correlations within the BO network (i.e., the B-B, B-O, and O-O) have been added together to produce a concentration weighted ''BO-BO partial'' structure factor, and the correlations within the AgI salt and the crossterms between the network atoms and the salt ions have correspondingly been added to a ''AgI-AgI partial'' structure factor and a ''BO-AgI partial'' structure factor, respectively. The BO-BO and AgI-AgI partials show, respectively, an intense and a weak peak at about 0.75 $Å^{-1}$, while the BO-AgI correlation has a dip at a similar Q value, as mentioned above. This indicates, as for the undoped glass, that the Ag^+ and I^- ions participate in crosslinking between neighboring BO segments. Note also that the BO-AgI partial shows almost no oscillations over the whole Q range, indicating that the silver and iodine ions are very weakly correlated to the BO network and that their positions are less well defined compared to silver ions in the undoped glass. Thus, two facts are evident from Fig. 7(b). First, it is mainly the density fluctuations within the BO network that causes the FSDP in $S(Q)$ and, second, the silver and iodine ions are present in the voids between the BO segments, without participating in the network formation. The relatively weak peak at about 0.75 $Å^{-1}$ in the AgI-AgI partial is interpreted as being due to correlations over the BO network, since the ''clustered'' BO network causes voids in the silver and iodine distributions which are likely to produce a weak prepeak in the correlations between the salt ions.

Figures 8(a) and 8(b) show the structure of the BO network and the distribution of silver ions in the undoped glass, and Figs. 9(a) and 9(b) show the corresponding BO structure and Ag^+ and I^- distributions for the highest doped glass. The figures show a 10-Å-thick slice of the two RMC configurations. By comparing Figs. 8(a) and 9(a) the dopant salt-induced expansion of the BQ network is clearly visible. The voids in the BO network of the doped glass [see Fig. 9(a)] are of relatively well-defined size (8 ± 3 Å) and the average distance over the voids corresponds well to the Q value of the FSDP ($2\pi/Q_1 \approx 8$ Å). Both the silver ions of the undoped glass [see Fig. 8(b)] and the silver and iodine ions of the doped glass [see Fig. 9(b)] seem to be rather homogeneously distributed and no AgI clusters of any significant sizes are observed in Fig. 9(b).

2. Short-range order

Figure 10(a) shows the partial pair correlation functions $G_{ij}(r)$ for $Ag_2O\text{-}2B_2O_3$. The first peak of the partials $G_{OO}(r)$ and $G_{AgO}(r)$ are relatively sharp and symmetrical around 2.4 Å, while the first peak of $G_{BB}(r)$ has a ''tail'' at large r, indicating that some of the B-O-B bond angles are close to 180°. Both $G_{AgB}(r)$ and $G_{AgAg}(r)$ show a very broad peak at about 3.1 Å, indicating a rather weak correlation between these atomic pairs. Here it may be instructive to compare the findings with the corresponding crystalline phase. We have then to compare with the silver tetraborate structure since there is unfortunately no structural determination of crystalline $Ag_2O\text{-}2B_2O_3$ reported. The structure of crystalline $Ag_2O\text{-}4B_2O_3$ contains many different Ag-B and Ag-Ag distances.[41] It is therefore not surprising that glassy $Ag_2O\text{-}2B_2O_3$ shows broad distributions of these pair distances. However, the shortest Ag-Ag distance for the crystalline structure of $Ag_2O\text{-}4B_2O_3$ is 3.69 Å, which is consid-

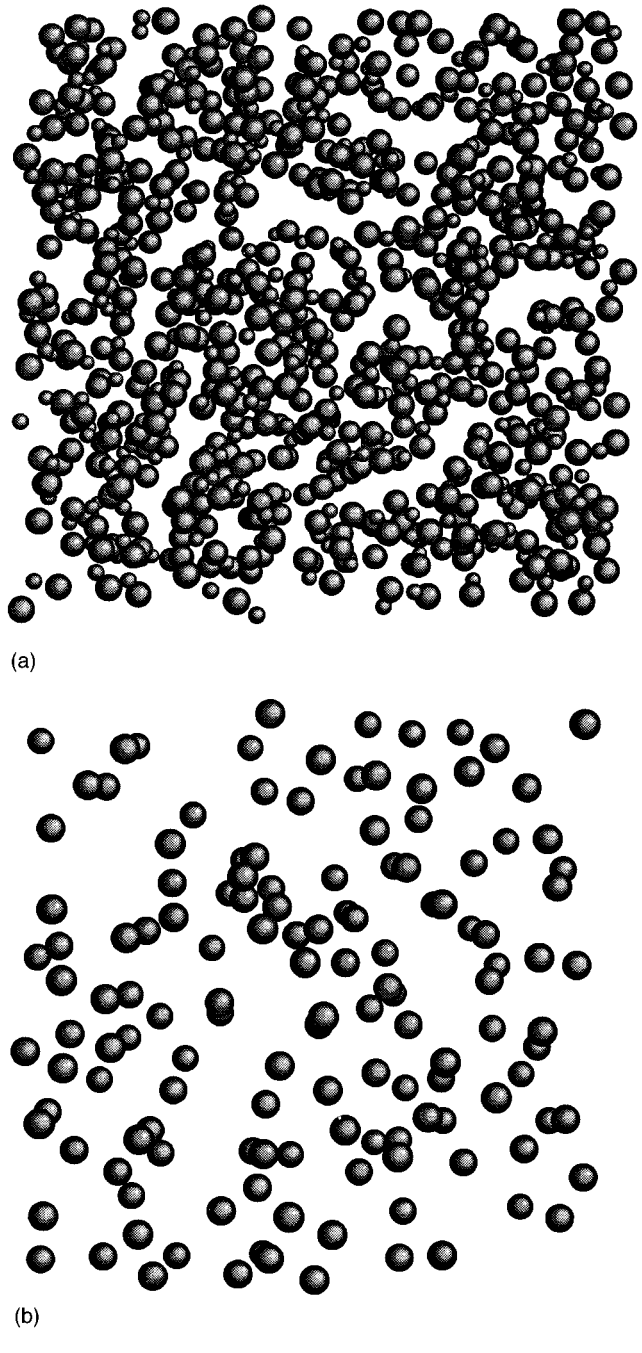

FIG. 8. A 10-Å-thick slice of the RMC configuration of Ag_2O-$2B_2O_3$. (a) shows the structure of the BO network and (b) the distribution of silver ions. The radii of the chemical components are B=0.5, O and Ag^+ = 0.8 Å.

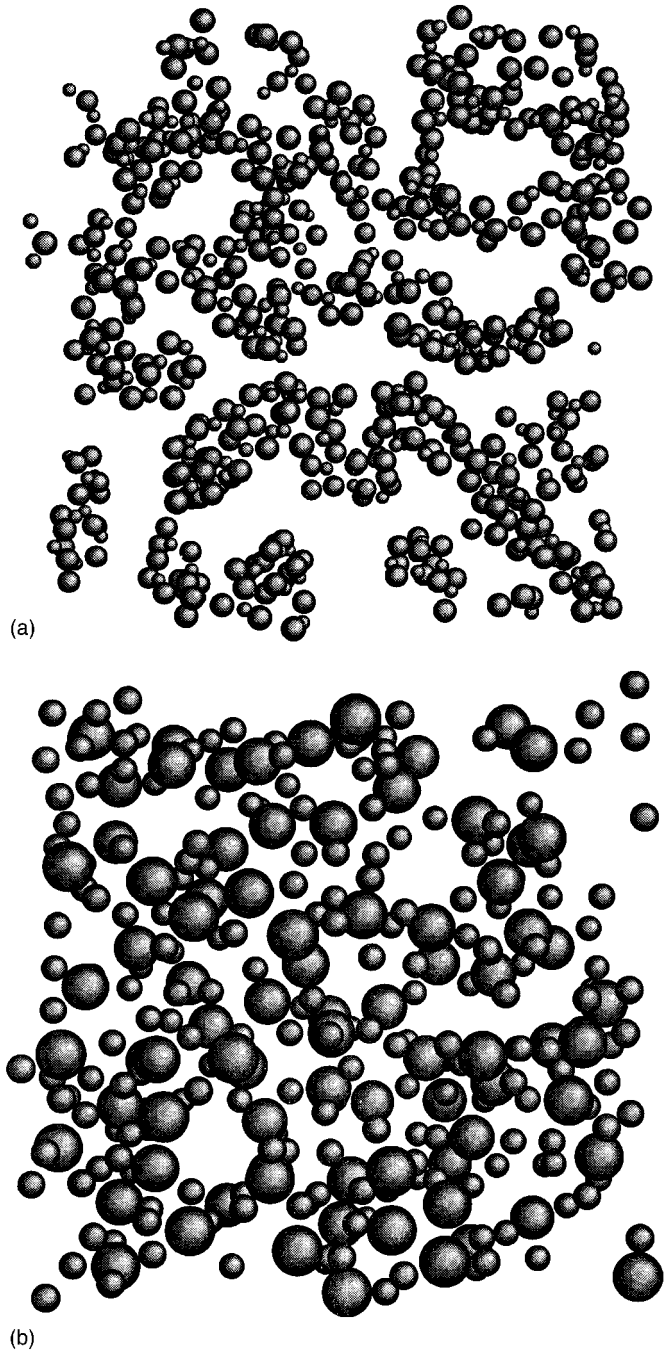

FIG. 9. A 10-Å-thick slice of the RMC configuration of $(AgI)_{0.6}(Ag_2O\text{-}2B_2O_3)_{0.4}$. (a) shows the structure of the BO network and (b) the distribution of silver and iodine ions. The radii of the chemical components are B=0.5, O and Ag^+=0.8, and I^-=1.6 Å.

erably longer than the main Ag-Ag distance found here for glassy Ag_2O-$2B_2O_3$. The coordination number of the first Ag-O peak, N_{AgO}, is estimated at 3.3, which is in good agreement with the value (3.7 ± 0.5) determined experimentally from neutron diffraction.[35] Figure 11(a) shows the distribution of Ag-O coordination numbers of the RMC model. From the figure it is evident that the distribution is wide and that many different coordinations exist.

The partial pair correlation functions of $(AgI)_{0.6}(Ag_2O\text{-}2B_2O_3)_{0.4}$ are shown in Fig. 10(b). It is evident from the figure that the first peaks in $G_{ij}(r)$, not involving I correlations, are very similar to the corresponding peaks of the undoped glass, although the nearest Ag-O and Ag-B correlations are less well defined and have lower coordination numbers. The partials which involve I correlations show no pronounced peaks, except for the nearest Ag-I distance, indicating that the iodine ions are very weakly connected to the BO network. The absence of any significant first I-I shell and also any second-neighbor Ag-I coordination shows that no larger AgI clusters are present in the structure. Thus, the

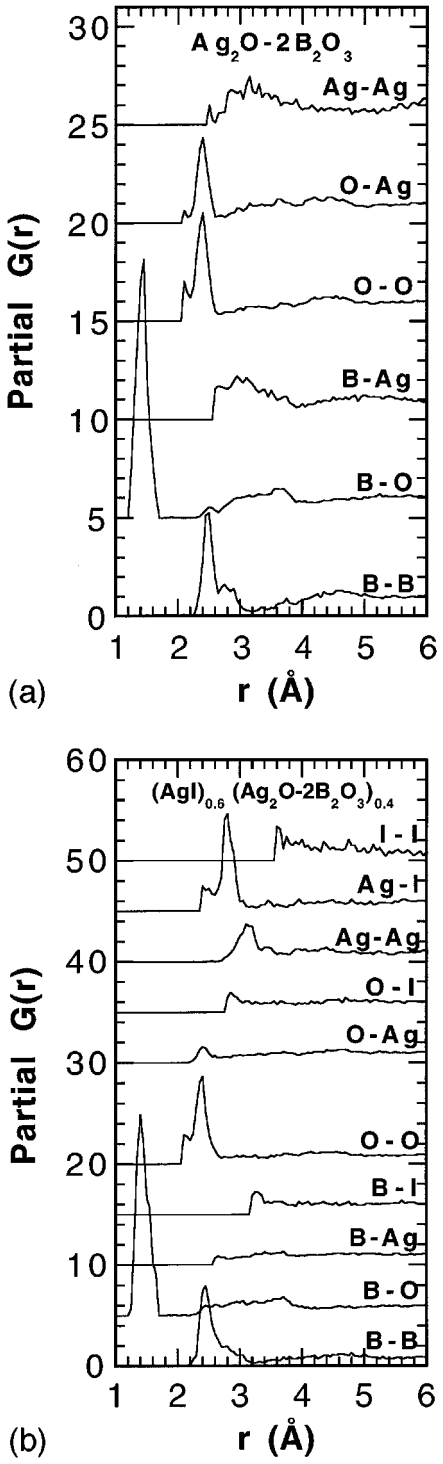

FIG. 10. Partial pair correlation functions, $G_{ij}(r)$, calculated from the RMC configuration of (a) Ag_2O-$2B_2O_3$ and (b) $(AgI)_{0.6}(Ag_2O$-$2B_2O_3)_{0.4}$. The upper curves have been shifted to higher values for clarity.

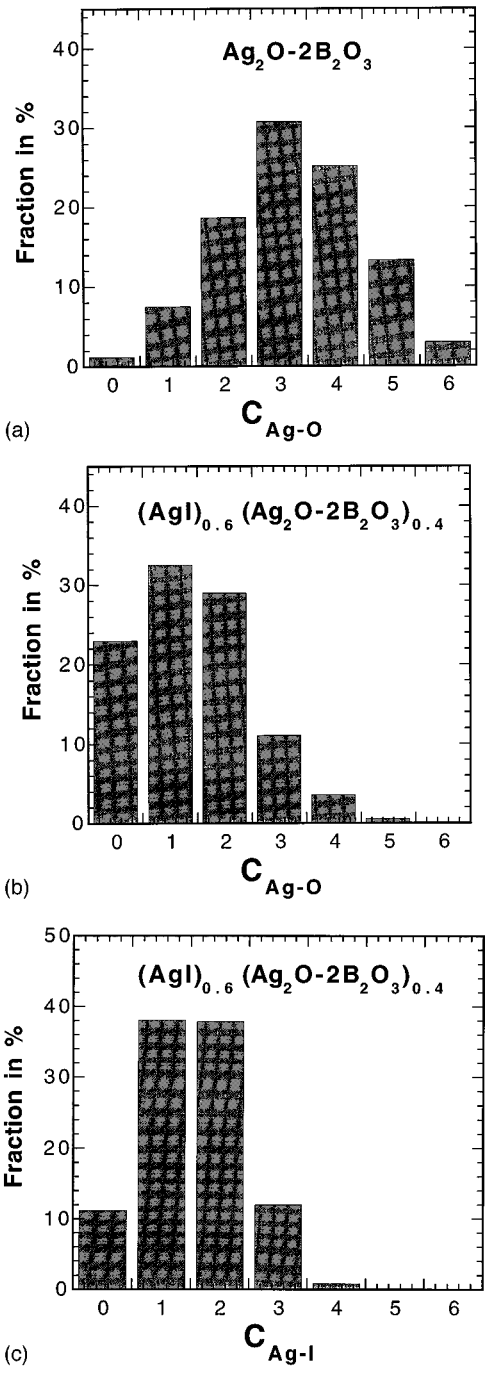

FIG. 11. Distributions of coordination numbers for (a) Ag-O in Ag_2O-$2B_2O_3$, (b) Ag-O, and (c) Ag-I in $(AgI)_{0.6}(Ag_2O$-$2B_2O_3)_{0.4}$.

observations made for the partial structure factors are seen also in the real-space correlations.

By comparing Figs. 10(a) and 10(b) it is found that the Ag-Ag correlation is nearly preserved for the doped glass, while the coordination numbers for the nearest Ag-O ($r<3.0$ Å) correlation are reduced to about a third of the value for the undoped glass. This implies that the iodine ions, introduced by the dopant salt, also affect the coordination of the Ag^+ ions from the network modifier. Thus, a large number of the Ag^+ ions, which in the case of the undoped glass are coordinated on average to 3–4 oxygens (of BO_4^- units), are for the AgI-doped glass coordinated to both I^- and BO_4^-. This is evident in Figs. 11(b) and 11(c) which show the distribution of Ag-O and Ag-I coordination numbers, respectively, of the RMC model. Furthermore, one can note that many different combinations of coordinations exist. Similar findings have been indicated by previous x-ray

diffraction[48] and NMR results.[49] The average coordination numbers of the nearest Ag-O ($r<3.0$ Å) and Ag-I ($r<3.2$ Å) distances are both estimated to be about 1.5 [see Figs. 11(b) and 11(c)].

VI. DISCUSSION AND CONCLUSION

Both the results obtained from the RMC simulations and the comparison of x-ray- and neutron-diffraction data show that the origin of the FSDP is mainly due to large density fluctuations within the B-O network [see Figs. 5(a), 5(b), and 7(b)]. Actually, this result is not very surprising if one takes into consideration that the highest AgI doping causes an expansion of the B-O network of about 60% while its short-range order is preserved. Thus, this large network expansion must give rise to large voids. The density fluctuations produced are likely to produce a prepeak similar to that found in the total neutron structure factor and the partial structure factors $S_{\mathrm{BB}}(Q)$, $S_{\mathrm{OB}}(Q)$, and $S_{\mathrm{OO}}(Q)$ obtained both from the RMC simulation and the initial HSMC simulation. The fact that even the starting configuration shows a FSDP (however at about 0.4 $\mathrm{Å}^{-1}$) indicates that the presence of a prepeak is a natural result of the large network expansion and the maintained connectivity. Furthermore, the experimental data (see Secs. IV A and IV C) exclude any explanation of the FSDP in terms of AgI clusters, because such clusters would have given rise to an enormously intense prepeak in the x-ray structure factor and an increasing intensity of the FSDP with increasing Ag scattering length. This conclusion for the AgI-doped glass is also in agreement with the results obtained from the RMC simulation (see Secs. V C 1 and V C 2), which showed that it is mainly the partial structure factors $S_{\mathrm{BB}}(Q)$, $S_{\mathrm{QB}}(Q)$, and $S_{\mathrm{OO}}(Q)$ that contribute to the experimentally observed FSDP at about 0.8 $\mathrm{Å}^{-1}$. Thus, the results indicate that the silver and iodine ions simply fill up the voids within the BO network without forming any AgI clusters of significant sizes. This is supported by the ''antiphase'' behavior of the salt-network partial structure factors in the Q region of the experimental FSDP [see Fig. 7(b)].

Most of the above-mentioned results concerning the intermediate-range order are, in fact, directly visible in the structures. In Figs. 8(a) and 9(a) it is seen that the BO network is formed into a ''double-chain'' structure similar to the diborate chains in crystalline borate phases, as was proposed by Cervinka *et al.*[50] In the doped glass the introduction of the silver and iodine ions cause an increased separation of the chain segments. The origin of the FSDP is clearly visible in the structure as an interchain ordering between neighboring chain segments. It is seen in Figs. 8(b) and 9(b) that the silver and iodine ions are relatively homogeneously distributed. Thus, the combination of Figs. 9(a) and 9(b) gives a picture where the borate chains run through a relatively homogeneous distribution of Ag^+ and I^- ions. The space between the borate chains seems to form pathways which are likely to be favorable for diffusion of Ag^+ ions.

In this section we would also like to conclude by giving structural ''pictures'' of the results obtained from the diffraction experiments and the RMC simulations of the Ag_2O-$2B_2O_3$ and $(AgI)_{0.6}(Ag_2O\text{-}2B_2O_3)_{0.4}$ glasses. Let us begin with the undoped glass, where the results indicated that the silver ions of the Ag_2O-$2B_2O_3$ glass are coordinated entirely to BO_4^- units. By comparing the nearest Ag-O (about 2.4 Å) and Ag-B (about 3.1 Å) distances, one can conclude that most of the Ag^+ ions cannot be coordinated to two oxygen atoms from the same BO_4^- unit, since this would require a nearest Ag-B distance of about 2.7 Å, provided that the Ag^+ ion is symmetrically coordinated to two oxygens in the same BO_4^- unit. Thus, for the undoped glass it appears that most of the Ag^+ ions bridge between different BO_4^- units. This result is in contrast to the first result of an extended x-ray-absorption fine-structure (EXAFS) investigation,[51] but in agreement with a later proposed structural model.[50] These findings, in combination with the large electronegativity of the Ag^+ ion, suggest that most silver ions form O-Ag-O bridges with significant covalent character between neighboring BO_4^- units. This causes an ordering of BO chain segments characterized by a relatively well-defined distance, given by B-O-Ag-O-B, between two neighboring borate chain segments. The interchain distance should correspond well to the observed characteristic intermediate distance of about 5 Å ($=2\pi/Q_1$) in the structure. Of course, this is an idealized and too ordered ''picture'' of the structure, on which a high degree of disorder should be superimposed (e.g., the results from the RMC simulation show that most of the Ag^+ ions crosslink between more than two BO_4^- units).

Let us now turn to the doped glass and focus on the structural effects of introducing the dopant ions. We note that the results for the $(AgI)_{0.6}(Ag_2O\text{-}2B_2O_3)_{0.4}$ glass showed that most of the Ag^+ are coordinated to both I^- ions and BO_4^- units and that the FSDP at about 0.8 $\mathrm{Å}^{-1}$ is a ''new'' peak in the sense that it is not the FSDP of the undoped glass that has been shifted to a lower Q value in the doped glass (see Fig. 1). Instead, it is obvious that the introduced dopant ions increases the intensity of a new FSDP, without changing its position (although the peak is not observable for the lowest salt concentrations). Thus, the experimental results indicate that a characteristic mean distance of about 8–9 Å ($=2\pi/Q_1$) develops continuously in the structure with increasing dopant concentration. The reason for this is likely to be that the silver and iodine ions participate in the crosslinking between neighboring chain segments, forming local B-O-Ag-I-Ag-O-B ordering similar to what has been suggested by Licheri *et al.*[42] The formation of such bridges should then push the diboratelike ''double chains'' apart and increase the distance between two neighboring segments to a mean distance corresponding to the position of the new FSDP, i.e., about 8–9 Å [see Fig. 9(a)]. For the highest doped glass it is probable that almost all the O-Ag-O bridges, present in the undoped glass, have been modified to O-Ag-I-Ag-O bridges, where, at average, every Ag^+ ion coordinate to 1.5 oxygens and 1.5 iodine ions (see Fig. 11). The above given structural ''picture'' also helps to explain why the silver and iodine ions form crystalline AgI for higher dopant concentrations, since even longer bridges would then be too weak to keep segments of the boron-oxygen network together. The excess AgI that is not introduced in crosslinks will then not be solvated in the boron-oxygen structure and will instead crystallize.

It is not established if the presence of well-pronounced diffusion pathways in the glass network is an essential struc-

tural feature for high ionic conductivity, although Fig. 9(a) shows that the space between the borate chains constitute clearly observable pathways for ion migration in the doped borate glass. However, similar pathways have also been found in highly conducting AgI-doped phosphate glasses,[27] which together with the present observations indicate that their presence may be favorable for ionic conduction. This would then support the diffusion pathway model[7,18,19] and the ideas of Tuller and Button,[22] i.e., that the ions of the dopant salt expands the network and gives rise to a more open structure suitable for ion conduction. It is evident from several independent aspects of the structural results obtained that the suggested cluster model for ion conduction[12–17] can be immediately rejected (see Secs. IV A, IV C, V C 1, V C 2). Some of the observed differences between the glass structures and the corresponding crystalline structures may also play important roles in the ion conduction, since the corresponding crystalline structures have negligible conductivities. In particular the significantly lower average total number densities (i.e., larger free volumes) and the presence of relatively short Ag-Ag distances in the glasses may be of importance, since they would both facilitate jump processes of silver ions along the found pathways. The increasing conductivity for increasing dopant concentration may partly be explained by the dopant ion-induced widening of the pathways. The expansion of these pathways is likely to cause the experimentally observed decrease in activation energy for ion migration, $E_a = E_b + E_s$, since the strain term E_s is directly related to the size of existing doorways. It is also possible that the electrostatic binding term E_b for the silver ions decreases due to the reduced interaction with oxygens when the I^- ions are introduced.

ACKNOWLEDGMENT

This work was financially supported by the Swedish Natural Science Research Council.

*Present address: Department of Physics and Astronomy, University College London, London WC1E 6BT, UK.

[1] C. A. Angell, in *Relaxations in Complex Systems*, edited by K. L. Ngai and G. B. Wright (National Technical Information Service, U. S. Department of Commerce, Springfield, VA, 1985), p. 3.
[2] C. A. Angell, Nucl. Phys. B **5A**, 69 (1988).
[3] C. A. Angell, J. Phys. Chem. Solids **49**, 863 (1988).
[4] C. Chiodelli, A. Magistris, M. Villa, and J. L. Bjorkstam, J. Non-Cryst. Solids **51**, 143 (1982).
[5] S. A. Feller, W. J. Dell, and P. J. Bray, J. Non-Cryst. Solids **15**, 21 (1982).
[6] A. Schiralidi, E. Pezzati, P. Beldani, and S. W. Martin, Solid State Ion. **18** and **19**, 426 (1986).
[7] G. Carini, M. Cutroni, A. Fontana, G. Mariotto, and F. Rocca, Phys. Rev. B **29**, 3567 (1984).
[8] L. Börjesson, L. M. Torell, and W. S. Howells, Philos. Mag. B **59**, 105 (1989).
[9] L. Börjesson, L. M. Torell, U. Dahlborg, and W. S. Howells, Phys. Rev. B **39**, 3404 (1989).
[10] C. A. Angell, Annu. Rev. Phys. Chem. **43**, 693 (1992).
[11] M. Tachez, R. Mercier, J. P. Malugani, and A. J. Dianoux, Solid State Ion. **18-19**, 372 (1986).
[12] M. Tachez, R. Mercier, J. P. Malugani, and A. J. Dianoux, Solid State Ion. **20**, 93 (1986).
[13] J. P. Malugani, M. Tachez, R. Mercier, A. J. Dianoux, and P. Chieux, Solid State Ion. **23**, 189 (1987).
[14] A. Fontana, F. Rocca, and M. P. Fontana, Phys. Rev. Lett. **58**, 503 (1987).
[15] A. Fontana, F. Rocca, and M. P. Fontana, Philos. Mag. B **56**, 251 (1987).
[16] C. Rousselot, M. Tachez, J. P. Malugani, R. Mercier, and P. Chieux, Solid State Ion. **44**, 151 (1991).
[17] C. Rousselot, J. P. Malugani, R. Mercier, M. Tachez, P. Chieux, A. J. Pappin, and M. D. Ingram, Solid State Ion. **78**, 211 (1995).
[18] T. Minami, J. Non-Cryst. Solids **73**, 273 (1985).
[19] M. D. Ingram, Philos. Mag. B **60**, 729 (1989).
[20] A. M. Glass and K. Nassau, J. Appl. Phys. **51**, 3756 (1980).
[21] D. Ravaine, J. Non-Cryst. Solids **73**, 287 (1985).
[22] H. L. Tuller and D. P. Button, in *Transport-Structure Relations in Fast Ion and Mixed Conductors*, edited by F. W. Poulsen, N. Hessel-Andersen, K. Clausen, S. Skaarup, and O. Soerensen (Risø National Laboratory, Roskilde, Denmark, 1985), p. 119.
[23] R. L. McGreevy and L. Pusztai, Molec. Simul. **1**, 359 (1988).
[24] D. A. Keen and R. L. McGreevy, Nature **344**, 423 (1990).
[25] M. Tachez, R. Mercier, and J. P. Malugani, Solid State Ion. **25**, 263 (1987).
[26] L. Börjesson and W. S. Howells, Solid State Ion. **40/41**, 702 (1990).
[27] J. Wick, L. Börjesson, R. L. McGreevy, W. S. Howells, and G. Bushnell-Wye, Phys. Rev. Lett. **74**, 726 (1995).
[28] G. Placzek, Phys. Rev. **86**, 377 (1952).
[29] R. W. James, *X-Ray Crystallography*, 5th ed. (Wiley, New York, 1953).
[30] T. E. Faber and J. M. Ziman, Philos. Mag. **11**, 153 (1965).
[31] L. Börjesson, Phys. Rev. B **36**, 4600 (1987).
[32] L. Börjesson and L. M. Torell, Solid State Ion. **25**, 85 (1987).
[33] W. S. Howells (unpublished).
[34] M. Howe, W. S. Howells, and R. L. McGreevy, J. Phys: Condens. Matter **1**, 3433 (1989).
[35] J. Swenson, L. Börjesson, and W. S. Howells, Phys. Rev. B **52**, 9310 (1995).
[36] G. Bushnell-Wye and R. J. Cernik, Rev. Sci. Instrum. **63**, 1001 (1992).
[37] A. H. Compton, Phys. Rev. **21**, 483 (1923).
[38] B. E. Warren and G. Marvel, Rev. Sci. Instrum. **36**, 196 (1965).
[39] G. Bushnell-Wye, J. L. Finney, J. Turner, D. W. Huxley, and J. C. Dore, Rev. Sci. Instrum. **63**, 1153 (1992).
[40] V. M. Nield, D. A. Keen, W. Hayes, and R. L. McGreevy, Solid State Ion. **66**, 247 (1993).
[41] J. Krogh-Moe, Acta Crystallogr. **18**, 77 (1965).
[42] G. Licheri, A. Musini, G. Pashina, G. Piccaluga, G. Pinna, and A. Magistris, J. Chem. Phys. **85**, 500 (1986).
[43] M. C. Abramo, G. Pizzimenti, and A. Consola, Philos. Mag. B **64**, 495 (1991).
[44] N. Metropolis, A. W. Rosenbluth, M. N. Rosenbluth, A. H. Teller, and E. Teller, J. Phys. Chem. **21**, 1087 (1953).
[45] F. Galeener, G. Lucovsky, and J. C. Mikelsen, Jr., Phys. Rev. B **8**, 3983 (1980).
[46] J. Lorösch, M. Couzi, J. Pelous, R. Vacher, and A. Levasseur, J. Non-Cryst. Solids **69**, 1 (1984).

[47] E. I. Kamitsos, A. P. Patsis, M. A. Karakassides, and G. D. Chryssikos, J. Non-Cryst. Solids **126**, 52 (1990).
[48] J. Krogh-Moe, Phys. Chem. Glasses **6**, 46 (1965).
[49] S. H. Chung, K. R. Jeffrey, J. R. Stevens, and L. Börjesson, Phys. Rev. B **41**, 6154 (1990).
[50] L. Cervinka, F. Rocca, P. Fornasini, and G. Dalba, J. Non-Cryst. Solids **150**, 140 (1992).
[51] G. Dalba, P. Fornasini, F. Rocca, E. Bernieri, E. Burratini, and S. Mobilio, J. Non-Cryst. Solids **91**, 153 (1987).